Space Science Reviews (2023) 219:69
https://doi.org/10.1007/s11214-023-01009-2

L'Ralph: A Visible/Infrared Spectral Imager for the Lucy Mission to the Trojans

D.C. Reuter[1] · A.A. Simon[1] · A. Lunsford[2] · H. Kaplan[1] · M. Garrison[1] · J. Simpson[1] · G. Casto[1] · Z. Dolch[1] · P. Finneran[3] · W. Grundy[4] · C. Howett[5] · P. Kim[1] · M. Loose[6] · T. Null[1] · F. Parong[1] · J. Rodriguez-ruiz[1] · P. Roming[7] · K. Smith[7] · P. Thompson[1] · B. Tokarcik[1] · T. Veach[7] · S. Wall[1] · J. Ward[8] · E. Weigle[9] · H. Levison[10]

Received: 27 June 2023 / Accepted: 29 September 2023 / Published online: 25 October 2023

Abstract
The Lucy Mission to the Trojan asteroids in Jupiter's orbit carries an instrument named L'Ralph, a visible/near infrared multi-spectral imager and a short wavelength infrared hyperspectral imager. It is one of the core instruments on Lucy, NASA's first mission to the Trojans. L'Ralph's primary purpose is to map the surface geology and composition of these objects, but it will also be used to search for possible tenuous exospheres. It is compact, low mass (32.3 kg), power efficient (24.5 W), and robust with high sensitivity and excellent imaging. These characteristics, and its high degree of redundancy, make L'Ralph ideally suited to this long-duration multi-flyby reconnaissance mission.

Keywords Trojan asteroids · Asteroids · Multi-spectral · Hyperspectral · Space mission

✉ D.C. Reuter
dennis.c.reuter@nasa.gov

1 NASA/GSFC, Code 693, Greenbelt, MD 20771, USA

2 American University, NASA/GSFC, Code 693, Greenbelt, MD 20771, USA

3 Jackson and Tull Inc., Beltsville, MD 20705, USA

4 Lowell Observatory, Flagstaff, AZ 86001 USA

5 Department of Physics, Clarendon Laboratory, Oxford University, Parks Rd., Oxford, OX1 3PU, UK

6 Markury Scientific, 518 Oakhampton St., Thousand Oaks, CA, 91361, USA

7 Southwest Research Institute, 6220 Culebra Rd., San Antonio, TX, 78228, USA

8 Newton-Engineering and Product Development, 5650 Rivertech Ct., Riverdale, MD, 20737, USA

9 Big Head Endian, LLC, 11785 181st RD, Burden, KS, 67019, USA

10 Space Sciences and Engineering Division, Southwest Research Institute (SwRI), 1050 Walnut St., Suite 400, Boulder, CO, 80302, USA

Abbreviations

A/D	Analog to Digital
ASIC	Applications Specific Integrated Circuit
AU	Astronomical Units
BHE	Big Head Endian
C&DH	Command and Data Handling
CCD	Charge Coupled Device
CDS	Correlated Double Sampling
DAC	Digital-to-Analog Converter
DN	Digital Number
DPSE	Differential Position Sensor Electronics
DPSS	Differential Position Sensor System
EGA	Earth Gravity Assist
FPE	Focal Plane Electronics
FOV	Field of View
FPGA	Field Programmable Gate Array
FSW	Flight SoftWare
FWHM	Full Width at Half Maximum
FWTM	Full Width at Tenth Maximum
GSFC	Goddard Space Flight Center
HK	Housekeeping
IFOV	Instantaneous Field of View
IPP	Instrument Pointing Platform
IR	Infrared
IRSM	Infrared Source Module
LEISA	Linear Etalon Imaging Spectral Array
LVF	Linear Variable Filter
LVPS	Low Voltage Power Supply
M4	Multi-Mission Mass Memory
MCE	Mechanism Control Electronics
MEB	Main Electronics Box
MLI	Multi-Layer Insulation
MVIC	Multi-spectral Visible Imaging Camera
NIR	Near Infrared
NIST	National Institute of Science and Technology
PSF	Point Spread Function
OVIRS	OSIRIS-REx Visible and Infrared Spectrometer
SIDECAR	System Image, Digitizing, Enhancing, Controlling, And Retrieving
SMM	Scan Mirror Mechanism
SMS	Scan Mirror System
SNR	Signal-to-Noise Ratio
SWIR	Shortwave Infrared
SwRI	Southwest Research Institute
TDA	Telescope Detector Assembly
TDI	Time Delay Integration
TIRS	Thermal Infrared Sensor
TVac	Thermal Vacuum
VIS/IR	visible/infrared

1 Introduction

Lucy, a multi-encounter mission to the Trojan asteroids in Jupiter's orbit, is the first mission to explore this class of objects. Launched on October 16, 2021, it will visit 8 Trojans over a 12-year period. The scientific rationale for Lucy and the overall mission planning are described in detail in Levison et al. 2021, and Olkin et al. 2021, and in several papers in this collection (Levison et al. 2024; Olkin et al. 2024). The Lucy mission is led by Principal Investigator Dr. Hal Levison of the Southwest Research Institute (SwRI) of Boulder, CO and is managed by SwRI and Goddard Space Flight Center in Greenbelt, MD. A core remote-sensing instrument on Lucy is L'Ralph, a visible/NIR camera and shortwave infrared spectral imager. The instrument's primary purpose is to measure surface characteristics, including geological processes, geomorphology, photometric properties, and surface composition. L'Ralph will also be used to measure the properties of comas (if they are present) and to obtain compositional measurements of rings and small satellites (again, if present). This paper describes L'Ralph and specifies its characteristics. L'Ralph is similar in concept to the Ralph instrument on the New Horizons mission (Reuter et al. 2008), however it has numerous science-based and operational improvements, and its performance is significantly better than New Horizons Ralph. Improvements of L'Ralph over NH Ralph include a much broader IR spectral range, the addition of onboard memory, and a scanning mirror that allows images to be taken without additional spacecraft motion. L'Ralph was provided by NASA's Goddard Space Flight Center (GSFC, Greenbelt, MD), however significant contributions were made by numerous entities throughout the US. L'Ralph also shares characteristics with the OSIRIS-REx OVIRS instrument (Reuter et al. 2018).

The L'Ralph instrument is mounted to the Instrument Pointing Platform (IPP) on the Lucy spacecraft (Levison et al. 2024, this collection). It has two elements, the Main Electronics Box (MEB), which provides the data and command interface between the instrument and the spacecraft and operates the instrument, and the Telescope Detector Assembly (TDA). The TDA consists of an imaging optical assembly, a scan mirror mechanism, the detectors, a passive thermal system for cooling the detectors as well as the assembly as a whole, and the calibration sources. The imaging assembly consists of a single telescope that feeds two sets of focal planes: 1) the Multi-spectral Visible Imaging Camera (MVIC), a visible to near-IR imager and 2) the Linear Etalon Imaging Spectral Array (LEISA), a short-wavelength IR spectral imager. To limit thermal background, the TDA is cooled to $<$ 195 K. The telescope uses an unobscurred, off-axis, three-mirror anastigmat design. The entire telescope assembly, including the three diamond-turned powered mirrors, is constructed from grain aligned 6061-T6 aluminum. The housing, excluding the attached covers but including the integral optical mounts, is fabricated from a single Al block. This combination of an all-Al structure and optics is lightweight, has uniform thermal expansion coefficients and is sufficiently thermally conductive that thermal gradients are not significant over the range of operating temperatures expected during the Trojan encounters (see Sect. 3.6 for the temperature ranges). These characteristics ensure that the optical performance of the instrument will meet requirements for all encounters. The highly baffled, 75-mm aperture, VIS/IR telescope provides ample sensitivity at all the encounters, while minimizing size and mass. The f/6 system's approximately 450-mm effective focal length offers a good compromise between photometric throughput and alignment stability. The mirrors are direct diamond turned off-axis aspheres, each with surface roughness below 6.0 nm RMS, fabricated by Coherent Inc. of Richmond, CA. In addition to an entrance baffle, stray light control is improved by using a field baffle at an intermediate focus between the secondary and tertiary mirrors, and by baffles near the exit pupil after the tertiary mirror. A dichroic beamsplitter

transmits IR wavelengths longer than 0.95 μm to LEISA and reflects shorter wavelengths to MVIC.

MVIC is composed of 6 independent CCD arrays (channels) on a single substrate. Each of the CCDs has 5000 (cross-track) × 64 (along-track) optically active pixels and they operate in time delay integration (TDI) mode. The channels are panchromatic (350 – 950 nm), violet (375 – 480 nm), green (480 – 520 nm), orange (520-625 nm), phyllosillicate (625 – 750 nm), and near IR (750-950 nm). TDI operates by synchronizing the along-track transfer rate of each of the CCD's rows to the relative motion of the image across the detector's surface. In this way, each spot on the object being imaged transfers from one row to the next without being smeared and the integration time is increased by the number of rows used in the TDI observation, allowing high signal-to-noise measurements to be made even on fast scans. Thus, very large format images are obtained as the spacecraft scans the MVIC field of view (FOV) rapidly across the surface. The single pixel instantaneous field of view (IFOV) of an MVIC pixel is about 28.8 microradians and the cross-track width covered is about 144 milliradians (∼8.25°).

LEISA is a wedged filter infrared spectral imager that creates spectral maps in the compositionally important 0.95 – 3.95 μm shortwave infrared (SWIR) spectral region. It images a scene through a wedged filter (or Linear Variable Filter (LVF), Rosenberg et al. 1994) placed about 100 μm above a Mercury Cadmium Telluride (HgCdTe) detector array. The LVF is fabricated such that the wavelength varies along one dimension, the along-track scan direction. LEISA forms a spectral map by scanning the FOV across the surface in a push-frame fashion. The frame rate is synchronized to the rate of the scan, so that a frame is read out each time the image moves by the IFOV. The difference between a LEISA scan and a TDI scan is that in LEISA the row-to-row image motion builds up a spectrum while in TDI the motion increases the signal over a single spectral interval. The single pixel IFOV of a LEISA pixel is about 40 microradians and the maximum cross-track width covered is about 41 milliradians (∼2.35°)

2 L'Ralph Science Overview

The full scientific rationale for the Lucy mission to the Trojans is given in detail in Levison et al. (2021, 2024) and will not be repeated at length here. Briefly, the Trojan objects were scattered into the L4 and L5 Lagrange points in Jupiter's solar orbit early in the Solar System's development. In essence they are the "fossils" of planetary evolution existing in "archeological sites" of the Solar System that will be visited for the first time by the Lucy spacecraft. The objects to be explored (in order, (3548) Eurybates, (15,094) Polymele, (11,351) Leucus, (21,900) Orus, and the (617) Patroclus/Menoetius binary) represent a wide range of sizes, spectral reflectances, rotation rates, and possible sources. It should be noted that both Eurybates and Polymele have recently discovered moons (Noll et al. 2020; Buie et al. 2022) that will also be observed. The first exploration of the Trojans is both scientifically and publicly exciting. It will provide invaluable insights into the origin of, and ongoing processes in, the solar system.

The L'Ralph instrument will play a leading role in this exploration. It directly addresses seven of the Level 1, or primary, mission requirements (Levison et al. 2021) connected to the surface composition of the Trojans and how that is related to the surface topography and impact history. L'Ralph/MVIC shall obtain visible/NIR multi-spectral images at spatial resolutions and areal coverages that will help identify the shortwave spectral slope and

the presence of species producing broadband spectral features (e.g., phyllosillicates and pyroxene) and their correlation with surface structures at sizes on the order of the expected cratering levels. L'Ralph/LEISA shall obtain hyperspectral maps at somewhat lower spatial resolution than MVIC, but still sufficient to identify correlations with geological features, including craters of the size expected to be found. These maps will cover the wavelength range of 0.95 to 3.95 μm (albeit with reduced sensitivity for $\lambda > 3.8$ μm) with a spectral full width at half maximum (FWHM) of 0.01 μm or less over the required 1 – 3.8 μm spectral range. This spectral range and resolution were chosen to achieve good sensitivity to the minerals, volatiles, and complex hydrocarbons that may be expected to be present (including, for example, H_2O (ice and mineral hydration feature), H_2S, CH_4, CH_3OH, SO_2 and NH_3), to characterize the CH_2 and CH_3 bands of aliphatic hydrocarbons, and to examine polycyclic aromatic hydrocarbons (PAHs). The LEISA spectral resolution elements are at least double sampled.

The targeted SNR for these observations is based on existing observations of outer Solar System objects. For example, organic molecules have been detected on the asteroid (24) Themis (Rivkin and Emory 2010, Campins et al. 2010), and on the satellites Iapetus and Phoebe (Dalle Ore et al. 2012; Cruikshank et al. 2008). In each case, the depths of the absorption bands are between 4% and 10% of the local continuum and cover 2 or more LEISA spectral resolution elements. Given this, spectra with SNR of 25 per spectral sample in the spectral range 3.2 to 3.6 microns will enable us to search for organics of the type and abundance present on these other bodies at greater than the 2-σ level in even the narrowest bands. A similar SNR in the 3-μm region will enable analyses that distinguish between H_2O ice and hydrated materials (e.g., Takir and Emery 2012) as well as determine phyllosilicate mineralogy, if phyllosilicates are detected (e.g., Takir et al. 2013). Spectra of Trojans themselves (Brown 2016) have also shown evidence of 4% or more absorption near 3.1 μm. Similarly, an MVIC SNR of 25 or greater will allow accurate retrievals of the spectral slope and broadband features corresponding to mineral absorption bands. In order to ensure sufficient margin to the SNR requirements, the albedo is assumed to be quite low (3% in the visible/NIR, 4% in the SWIR). This, combined with the fact that, to avoid illumination phase changes during an observation and to carry out multiple observations with all the Lucy instruments, the Level 1 observations are made either before or after closest approach when the solar phase angle ranges from a maximum of 82 degrees (Polymele) to a minimum of 54 degrees (Orus) and, finally, that there are limits placed on integration time to avoid spacecraft and IPP pointing drift smear, makes the SNR requirement a very strong driver on L'Ralph sensitivity.

L'Ralph's MVIC and LEISA reflectance maps will allow us to address many questions pertaining to the composition of the Trojans. Such as what is the spatial variability and scale size of surface features? What is the surface distribution of the various species? Are there areas of pure frost and mixed areas? Are there more complex species in selected regions of the surface? Is there a connection between geology and composition? Can we see the effects of space weathering in areas where collisions have exposed sub-surface material? Answers to these questions will significantly advance our understanding of the processes that occurred throughout the outer regions of our solar system during its formation and of the ongoing chemical and physical processes that are occurring there now. Figure 1 shows some Earth based spectra of Trojan objects and other small bodies. As is evident from this figure, there is a wealth of information to be gleaned from in-situ observations of this spectral region even from globally averaged spectra.

In addition to the Level 1 objectives, L'Ralph will address numerous Level 2 measurement goals. These include: MVIC and LEISA observations of Trojan moons if they are

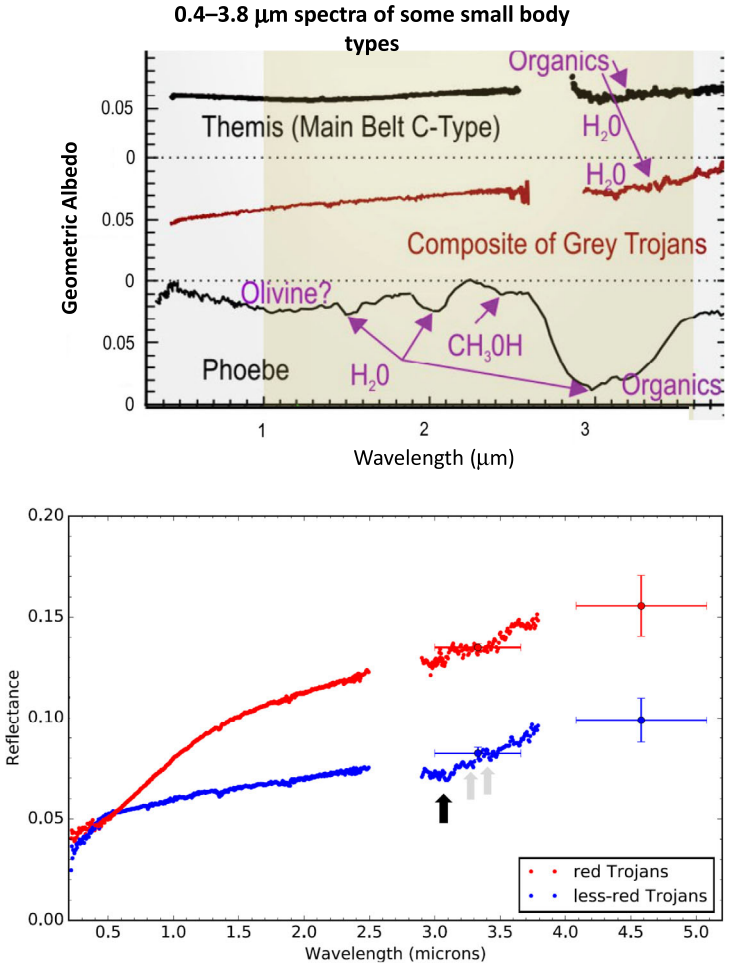

Fig. 1 Reflectance spectra of some small body objects (top) and Earth based spectra of red and less red Trojan object (bottom, Levison et al. 2021). As may be seen in these images, the hyperspectral measurements in the spectral range of 1 – 3.8 µm combined with multispectral measurements in the 0.4 to 0.9 µm regions are well suited to determining surface composition

found (two already have been), higher spatial resolution MVIC observations of some areas during the time near closest approach, higher spatial resolution LEISA observations over a limited spectral range during the time nearest closest approach, and MVIC and LEISA searches for a "coma" of volatile material in the time available before and/or after the Level 1 observations and closest approach. Table 1 summarizes the science objectives that determined the L'Ralph design, the measurement strategies that address these objectives and the derived instrument performance requirements. Note that the required spatial resolution for LEISA is dependent on the size of the Trojan and varies from 1 km for Polymele to 5 km for Patroclus. This is because the required resolution is set by the need to have a high probability of being able to measure a change in composition within resurfaced areas younger than 100 million years as predicted by cratering models.

Table 1 Science Objectives and Derived Instrument Requirements

Science Objective	Measurement Strategy	Derived Instrument Requirements			
		Spectral coverage	Resolution	Image Quality	Signal-to-noise
Determine the global distribution of compositional units.	Color images spaced by 1/6 to 1/3 of a rotation over a full target rotation.	No additional requirements	N/A	No additional requirements	No additional requirement
Search for compositional anomalies resulting from freshly exposed material.	Color images of an area $\geq$ 700 km^2 or 80% of the sunlit surface (whichever is less) capable of resolving features $\leq$ 1.5 km in size. Color images of an area $\geq$ 150 km^2 capable of resolving features $\leq$ 600 m in size	375 – 480 nm 480 – 520 nm 520 – 625 nm 625 – 750 nm 750 – 900 nm	85% of signal from 480-520 nm 91% of signal from 520-625 nm 91% of signal from 625-750 nm 87% of signal from 750-900 nm	Enclosed energy >54%; 50 mRad >83%; 76 mRad >91%; 168 mRad >98.2%; 242 mRad	SNR > 25 Scan 12 mrad target Distance = 5.7 AU I/F = 0.0014 Distance = 5.2 AU I/F = 0.005 1.2 s Maximum integration time No saturation on a scan for I/F a factor of 16 greater
Map the surface composition of the Trojan objects	Spectroscopic images shall detect features with relative spectral depth $\geq$ 4% and spectral width of $\geq$ 70 nm in the spectral range 1.0–3.4 microns, when the object spans multiple spatial resolution elements. Spectroscopic images shall cover a spectral range 1.0–3.8 microns Spectroscopic images spaced by 1/6 to 1/3 of a rotation over a full target rotation	1.0 – 3.8 μm	$\Delta\lambda \leq$ 10 nm (Full Width Half Maximum) in 1.0 to 3.4 range μm	No additional requirement.	SNR > 25 for spectral features of FWHM of 70 nm in the range 1.0-3.4 um Scan 12 mrad target Distance = 5.7 AU I/F = 0.0019 Distance = 5.2 AU I/F = 0.0068 1.5 s Maximum integration time No saturation on a scan for I/F a factor of 13 greater
Search for compositional anomalies resulting from freshly exposed material	Spectroscopic images with a combination of spatial resolution (r) and areal coverage (A), where A is 25% of the object's area, that together satisfy the condition $r \leq 2(A/A_0)^{\alpha}$ km where $\alpha = 0.473$, $A_0 = 1470.6$ km^2.	No additional requirement	No additional requirement	Enclosed energy >55%; 136 mRad >82%; 204 mRad >91%; 312 mRad >98.2%; 1020 mRad	No additional requirement.

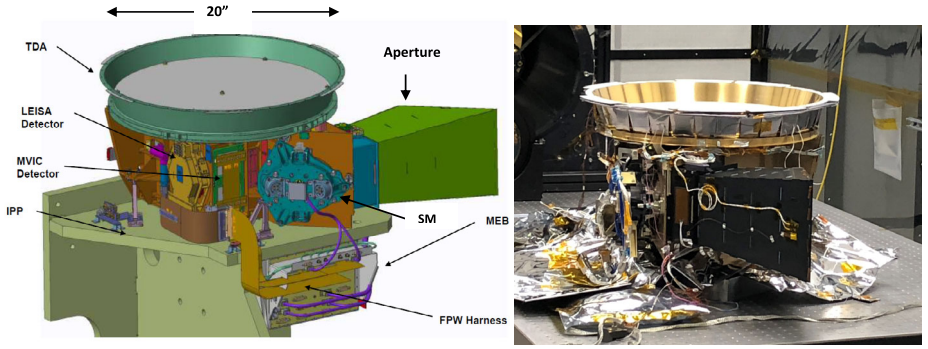

Fig. 2 Left) Model of the L'Ralph instrument mounted on the IPP. This shows both the TDA and the MEB with principal components labeled. (Right) Picture of the L'Ralph TDA, before the addition of most of the multi-layer insulation (MLI)

3 OPTO-Mechanical Design

Figure 2 shows a model of L'Ralph and a picture of the assembled instrument before addition of the final MLI. The major elements are labeled in the model. The mass of the instrument is 32.3 kg and the operational power is 24.5 Watts, both well within their allowable values (35.5 kg and 30 W, respectively). As shown in Fig. 2, L'Ralph has two main assemblies, the telescope detector assembly (TDA) and the Main Electronics Box (MEB). Both assemblies are mounted to the Instrument Pointing Platform (IPP). The TDA consists of the scan mirror assembly, the telescope optical elements, the baffling, the MVIC and LEISA focal planes, the two-stage passive radiator that cools the focal planes, the filament and blackbody calibration sources, and the solar calibrator. The TDA is mounted to the IPP by thermally isolating titanium flexures. Modeling done using results from instrument and spacecraft level thermal vacuum testing predict that during the Trojan encounters, the temperature of the TDA (not including the LEISA detector) will be between 160 and 200 K. The temperature of the electronics box, which is mounted directly to the IPP but thermally isolated from it, is predicted to be between 260 and 305 K. The low temperature of the TDA reduces the conductive and radiative thermal load on the focal planes. It also limits the background signal at the long wavelength end of LEISA. The inner stage of the externally mounted passive radiator cools the LEISA detector to < 115 K. The outer annulus maintains the MVIC CCDs at temperatures below 200 K. The 75 mm aperture, 450 mm focal length, f/6 optical system meets its spatial imaging requirements over the $8.25° \times 0.94°$ MVIC field of view and the $2.35° \times 3.37°$ LEISA FOV. The instrument parameters for L'Ralph are summarized in Table 2. Figure 3 shows a model of the TDA interior with a ray-trace diagram. Figure 4 shows a more detailed internal raytrace including the arrangement of scattering baffles and image stops.

3.1 The MVIC Focal Plane

The MVIC focal plane assembly, which was provided by SwRI, San Antonio TX, consists of a customized front side illuminated CCD array, provided by STA Inc., San Clemente, CA, mounted to a heat sink plate and placed directly behind a "butcher block" filter assembly. The array has six identical 5024-pixel TDI CCDs (5000×64 pixel photoactive area) on a single substrate. The extra 24 dark pixels (12 on each side of the 5000-pixel optically

Table 2 L'Ralph Instrument Parameters

Mass: 32.3 kg
Power: 24.5 Watt (maximum)
Telescope Aperture: 75 mm
Focal Length: 451.4 mm
f/#: 6
MVIC: Six Time Delay and Integrate (TDI) arrays
One 5024 × 64 Pixel Panchromatic TDI CCDs (350 – 950 nm)
Five 5024 × 64 Pixel Color TDI CCDs
Violet (375 – 480 nm)
Green (480 – 520 nm)
Orange (520 – 625 nm)
Phyllosilicate (625 – 750 nm)
Near-IR (750 – 900 nm)
Each CCD may be operated with 64, 32, 16, 8 or 4 TDI rows
13μm × 13μm pixels
Single pixel Field of View: 28.8 μrad × 28.8 μrad
TDI array FOV: 8.25° × 0.105°
Focal plane temperature: <200 K
Minimum TDI integration time (4 TDI, 7.2 msec rate): 27.8 msec
Maximum TDI integration time (64 TDI, 0.65 sec rate): 42 sec
LEISA: 2048 × 2048 element HgCdTe array operated in pushbroom mode.
18μm × 18μm pixels
Single pixel Field of View: 40 μrad × 40 μrad
FOV: 2.35° × 3.37° (1024 cross-track, 1472 along track)
Focal plane temperature: <115 K
Spectral range: 0.95 – 3.95 μm (1.0 – 3.8 μm required)
Spectral resolution: variable; < 10 nm
Frame rate: 0.38 sec to 21 sec (for 512 × 1472 pixels)
Minimum frame rate (10 × 1472 pixels): 20 msec

active region) are used to clear any residual charge in the serial readout before the optically active pixels are read out. The cross-track dimension of 5000 elements allows images to be taken that meet the spatial resolution requirements for all encounters, including the Patroclus-Menoetius binary if the two objects are displaced from each other in the cross-track direction, including pointing uncertainties. All MVIC pixels are 13 × 13 μm^2 which, given the optical properties above, corresponds to a single pixel IFOV of 28.8 × 28.8 μrad^2.

The filter, which was provided by VIAVI Solutions, Santa Rosa, CA, is mounted about 500 microns above the surface of the array. It has six segments, five with the passbands described in Table 2 placed directly over the five CCDs forming the color segment of MVIC. The remaining CCD is overlain by a clear filter so that the focus position is the same for all six arrays. The scan mirror is used to scan the image of each segment of the surface across the focal plane in a pushbroom fashion. As Fig. 5 illustrates, the clocking rate of each 5024-pixel row is determined by the scan mirror rotation rate so that a row charge transfer occurs each time the image has moved a pixel width. Each CCD has two outputs, one on each side of the cross-track serial readout, which allows faster readouts, and thus

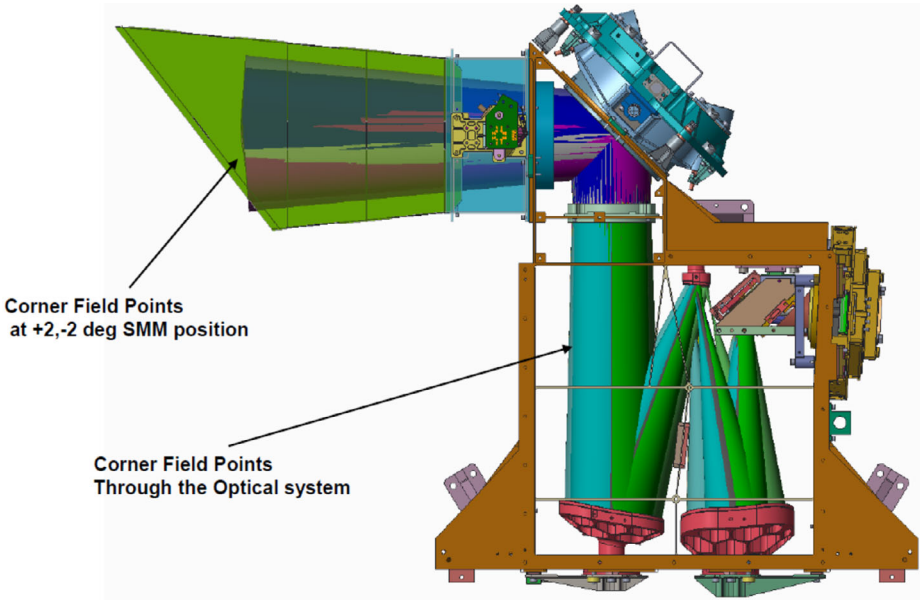

Fig. 3 Interior of the L'Ralph TDA showing the light path at the +2 degree and −2 degree positions of the scan mirror (+4 and −4 degrees of image motion)

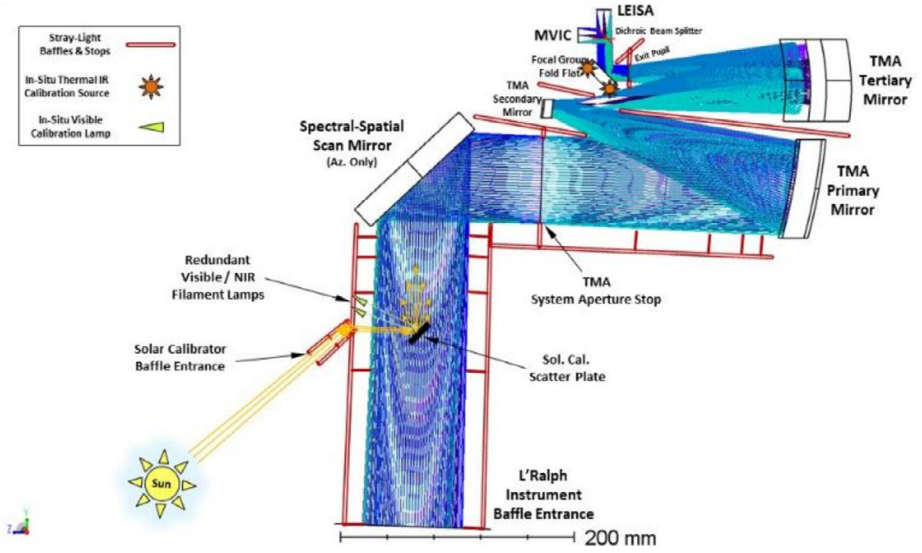

Fig. 4 Schematic of the interior of the TDA showing the optical elements and the baffle structures. The solar calibrator entrance, the position of the internal filament calibrator lamps, and the position of the thermal IR calibration sources are also shown

higher scan rates, than if there were only 1 output. Figure 5 shows an example of a TDI using 32 along-track rows. In L'Ralph, each CCD may be independently commanded to

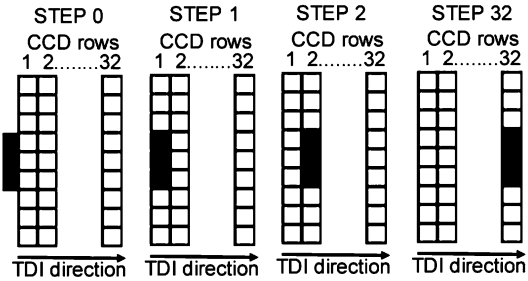

Fig. 5 Illustration of TDI in operation using 32 rows as an example. In step 0, a target is about to enter the field of view of a TDI array. In step 1, the image of the target has moved a single pixel width into the first row of the array. In step 2, the charge is transferred to the second row of the array and integration continues. A new target has moved into row 1. The next charge transfer occurs when the image of the target has moved another row. In step 32, the target has moved 32 rows, with the charge being transferred each time the image moves another row. At the next charge transfer, the charge in row 32 is transferred to a serial column for pixel readout. In L'Ralph,, each CCD may be independently commanded to use either 64, 32, 16, 8 or 4 along-track rows for TDI

use either 64, 32, 16, 8 or 4 along-track rows but, since the last row is shielded from light, there are 63, 31, 15, 7 and 3 optically active rows, allowing each channel to have a different integration time at a given scan rate. This allows data to be taken in all 6 channels in a single scan while maintaining good signal to noise ratios in the channels with lower illumination levels but not saturating in the channels with higher illumination levels. The minimum time between row transfers is 7.2 millisec, which gives a maximum scan rate of 28.8/0.0072 $\sim$ 4000 μrad/sec which, for a 4 row TDI, corresponds to an integration time of 0.0216 sec and 0.4536 sec for a 64 row TDI. This scan rate will be used for observation taken at lower solar phase angles. For most of the encounters the Level 1 data is obtained at relatively high phase angles requiring longer integration times and scan rates of about 1000–3000 μrad/sec will be used.

3.2 The LEISA Focal Plane

The LEISA focal plane assembly was provided by Newton Engineering and Product Development, Riverdale, MD. It consists of an HgCdTe H2RG detector array mounted to a heat sink with an LVF (also called a wedged filter or a linear etalon) directly over the array. The detector, which has a long wave cutoff wavelength of $\sim$3.85 μm, was supplied by Teledyne Imaging Sensors (TIS) of Camarillo CA. It is a 2048 $\times$ 2048-pixel array and each pixel is 18 $\times$ 18 μm^2 in area. The detector is read out using up to 32 outputs, each of which corresponds to a 64-pixel (along-track) $\times$ 2048-pixel (cross-track) section of the array. The HgCdTe was grown on a CdTe substrate using Molecular Beam Epitaxy (MBE) to provide good lattice matching and low dark currents. The detector was bump bonded to a standard multiplexer and the resulting hybrid was mounted to molybdenum pad. This process reduces mechanical stress induced during cooling to operational temperature. It is estimated that the assembly can safely undergo at least 1000 thermal cycles. The LEISA array is back illuminated, but, as is a standard practice, the substrate has been thinned so that the photo-active active area of the array is close to the surface (see, e.g. Beletic et al. 2008).

The filter, supplied by VIAVI Solutions. of Santa Rosa CA, consists of three segments covering 0.95–1.644 μm, 1.53–2.64 μm, and 2.55–3.99 μm respectively, which cover slightly

more spectral range than the 1–3.8 μm requirement. In all segments, the transmitted wavelength varies close to linearly with position in the along-track direction. The three segments were bonded together to form a single filter element. This filter was, in turn, bonded into a holder and mounted such that the filter surface is less than 100 μm above the surface of the array. To meet the Lucy spectral and spatial coverage requirements, only 23 detector outputs are needed, with 1024 cross-track pixels in each output. The filter holder covers most of the remaining pixels in the array to reduce possible crosstalk and scattered light. The wedged filter effectively makes the pixels in each cross-track column of the array responsive to only a narrow wavelength (<10 nm) band, so that in concept, when 23 outputs are used, the focal plane may be considered as consisting of 1472 (23 × 64) adjacent narrow band filters. As with MVIC, the image is scanned over the LEISA focal plane by the scan mirror motion with the frame rate synchronized to the scan rate. The refractive index of the array is approximately 2.7 so that the total optical path between the filter and photo-active area of the array is about 100 μm. When the focus position is optimized between the array and filter surface, the f/6 beam spreads about 0.5 pixel.

LEISA may be operated in two modes: correlated double sample (CDS) mode or raw mode. In CDS mode, the reset voltage level of each pixel is subtracted from the voltage read out at the end of the integration time, and that difference is stored in instrument memory. This is the typical mode used for science scans. In raw mode, both the reset voltage level and the voltage read out at the end of the integration time are stored for each pixel. This mode is used for some calibration collects. In addition, when data is stored in spacecraft memory, it can either be on a pixel-by-pixel basis or in the form of 2-pixel × 2-pixel "superpixel" sums. Superpixeling reduces spacecraft data volume by a factor of 4 and it is the standard process used for LEISA scans. The effective IFOV in this format is 80 μrad × 80 μrad and scans are planned accordingly. Note, however, that the data stored in instrument memory is still at the single pixel 40 μrad × 40 μrad level. For the planned Trojan scan, the required FOV of LEISA covers 512 (cross-track) × 1472 (along-track) pixels and the minimum integration time when reading this out is ∼0.38 seconds. However, shorter integration times may be obtained when reading out fewer than 512 cross-track pixels.

3.3 Scan Mirror System

The Scan Mirror System (SMS) is comprised of the redundant Mechanism Control Electronics (MCE) cards in the MEB, the Scan Mirror Mechanism (SMM) located on the Telescope Detector Assembly, and the redundant Differential Position Sensor System (DPSS) sensors (located on the SMM) and electronics (located on the exterior of the MEB). The SMM is a single axis flexure- based device capable of positioning the 140 mm × 100 mm open aperture scanning mirror through a ±2° range of physical motion to accommodate the ±4° line-of-sight scan requirements. The SMM employs e-beam welded flexural pivots to support the scan mirror with respect to the fixed base structure. Voice coil actuators provide electromotive force that rotates the mirror. Supported by three kinematic mounts (Ti-6-4 blade flexures), the SMM is oriented in a 2-2-2 configuration (three tangential bipod flexures spaced 120 degrees apart about a circle) centered on the central ray of the aperture. Fixed sides of the flexures are supported by a housing providing a mechanical interface to the instrument optical housing. The housing also acts as a protective environment for handling, transport, and test set ups.

The DPSS is an eddy current differential position sensor system provided by Blue Line Engineering which provides angular position knowledge of the SMM. This subsystem is

comprised of a pair of redundant sensor heads and redundant Differential Position Sensor Electronics (DPSE) boxes mounted externally to the MEB. The sensor heads provide inductive single axis sensing provided by pair of sensor heads on the SMM. The DPSE provides the interface between the MCE and sensor heads for sensor head power and the return analog position signal back to the MCE.

The redundant Field-Programmable Gate Array (FPGA) based MCE cards housed in the MEB provide the communication, control, telemetry, and power connectivity between the SMS and the rest of the L'Ralph instrument. Functionally, the MCE performs closed-loop control of the SMM with filtering and compensation parameters that can be uploaded to fine tune the system, necessary for achieving the highest performance. A Digital-to-Analog Converter (DAC) provides an analog signal to a linear power amplifier to drive the mirror actuators. The MCE is capable of commanding various scan rates from various start and stop scan positions including staring at specified position locations for instrument alignment. The MCE controls the SMM through a DAC and power amplifier/current driver. Scans are specified by three parameters: the scan rate, end-of-scan location, and a duration to dwell at end of scan before declaring the scan to be complete.

The SMS can scan at a maximum rate of 70 mrad/s, however that rate is only used for repositioning the mirror. The scan rates used for imaging typically range from 2 – 4000 μrad/sec with the rate controlled to better than 10 μrad/sec and the position known to better than 5 μrad. For MVIC the range of scan rates that correspond to the allowed integration times is 40 μrad/sec to 4000 μrad/sec. For LEISA the range of scan rates that correspond to the allowed integration times for 512 crosstrack pixels is 2 μrad/sec to 210 μrad/sec.

3.4 Inflight Calibration Sources: The Filament Calibrator, the Miniaturized Blackbody Calibrator, and the Solar Port

L'Ralph has three onboard calibration sources to provide a means to monitor the radiometric stability of the instrument, one is a solar port while the other two, a filament calibrator and a miniaturized blackbody calibrator, are electronically activated (see Fig. 4). These sources were not expected to provide absolute calibration. In flight, the absolute calibration of both MVIC and LEISA will be monitored by observing stellar sources. The solar port uses an input aperture, which is a tube mounted to the L'Ralph input baffle pointing about 43 degrees off axis from the primary aperture to obtain the calibration signal. When pointed at the sun, it allows solar radiation to strike a spectralon scatter plate that is placed in front of the scan mirror. The plate scatters light over a wide enough range of angles that it fills the entrance pupil (the System Aperture Stop (see Fig. 4)) and provides illumination over the entire FOV of both the MVIC and LEISA focal planes. Because it is solar illumination, it provides signal over the entire spectral range of both MVIC and LEISA when appropriate integration times are used. In ground testing, the solar calibrator was illuminated with a laser with similar power and angular spread as the sun at 5.2 AU to verify the signal obtained under those conditions was sufficient to provide adequate signal-to-noise ratio for calibration (SNR$>$50). The solar calibrator was not further calibrated during thermal vacuum testing because it was not being used for absolute calibration. The optical properties of spectralon can be affected by exposure to solar UV radiation, however, the scatter plate is well shielded from UV exposure, and only sees solar radiation during solar calibration. Also, since it is known that the changes in spectralon properties are associated with contamination (e.g. Leland and Arecchi 1995), significant effort was made to avoid contamination. The scatter plate is also shielded from cosmic radiation as well. Since use of the solar calibrator involves pointing the spacecraft, calibration operations that employ it will be done on an occasional basis. However, the

filament and blackbody calibrators will be used to monitor the calibration on a much more frequent cadence. Thus, during encounters, the radiometric stability of the instrument will be determined by frequent filament and blackbody measurements, complimented by less frequent solar calibrations and verified by even less frequent stellar calibrations.

The filament calibration source is a set of four small tungsten lamps (Chicago miniature, CM715) contained within an enclosure that is also mounted to the input baffle which illuminates the same scatter plate as the solar port. The four bulbs are divided into two pairs of two bulbs each to provide a redundant system. The filaments operate at a temperature of $\sim$ 2500 K at their maximum power level, providing usable signal over the entire LEISA spectral range and to the panchromatic and three longer wavelength color bands of MVIC. The miniaturized blackbody calibrator consists of a set of 4 elements, each of which contains 4 small silicon rectangles that can be heated to about 800 K. This is warm enough to provide usable radiance to LEISA at wavelengths longer than about 2.5 μm. Because this is not warm enough to produce usable signal for MVIC, the sources are located after all optical elements, very near the cold shield for the LEISA focal plane. As with the filaments, the 4 sources are powered as two redundant pairs of two sources each, so there are 16 total miniaturized blackbodies, divided into two sets of 8. The blackbody and filament calibrators were radiometrically calibrated with NIST traceable sources at several power settings during thermal vacuum testing. The filament and blackbody calibrations sources are the same as used on OVIRS, though in a different location, and have shown better than 2% stability during the first two years of that mission (Simon et al. 2018) and continue to be stable at that level 4 years later. The stability of these electronic sources will be monitored using the solar calibrations and the stellar calibrations.

3.5 Electronics

The L'Ralph MEB consists of a chassis containing ten boards all connected to a backplane: one IR focal plane electronics (FPE) card containing two redundant sides (the FPR-IR card); one CCD FPE card containing two redundant sides (the FPE-vis card); two redundant command and data handling (C&DH) cards; two redundant low voltage power supply (LVPS) cards; two redundant multi-mission mass memory (M4) cards; and two redundant mechanism control electronics (MCE) cards. All boards are contained within the MEB mounted directly to the IPP below the TDA. Two differential position sensor electronics (DPSE) boxes are mounted to the outside of the chassis. The MEB does not have temperature control electronics but does have survival heaters and temperature sensors.

The L'Ralph FPE boards in the MEB provide clocking and biases to the CCD and the H2RG, read out the analog image data from the arrays, amplify the signals from the arrays, and perform the 16 bit A/D conversion of the data using System Image, Digitizing, Enhancing, Controlling, And Retrieving (SIDECAR) Applications Specific Integrated Circuits (ASICs) (see, e.g. Loose et al. 2005). The L'Ralph FPE-IR design and SIDECAR operating process are near copies of what was used for the H1RG array on OVIRS which has been operating flawlessly since launch. The difference between the OVIRS operation and the L'Ralph operations is that on OVIRS eight 512-pixel long, 64-pixel wide, data channels were read out while on L'Ralph 23 1024-pixel long, 64-pixel wide, data channels were read out. The SIDECAR can support 32 2048-pixel long, 64-pixel wide, channels. The L'Ralph FPE-vis design is also based on the OVIRS application. The FPEs were provided by Jackson & Tull. The C&DH board interprets the commands, performs the A/D conversion of the low-speed engineering data, and provides both the high-speed

imaging data interface and the low-speed housekeeping (HK) data interface. It also performs the programmable pixel summing and correlated double sampling functions. The LVPS converts the 28 V spacecraft power to the various voltages required by L'Ralph, including those supplied to the settable calibration sources. The MCE controls the scan rate of the mirror and senses its position. Each of the redundant M4 cards contains 256 Gbits of nonvolatile memory in total. The MCE was provided by GSFC while the rest of the MEB boards were provided by SwRI. SwRI also provided the MEB enclosure. Flight Software (FSW) controlling the C&DH was provided by Big Head Endian (BHE) LLC. The FSW that controls the SIDECARs in the FPEs was provided by Markury Scientific.

In a long duration mission such as Lucy, reliability of the electronics is of paramount importance, particularly for a core instrument that addresses many Level 1 objectives. As is standard practice, the dosage levels of various radiation elements (e.g. Total Ionizing Dose (TID) in Silicon, Solar Proton Fluence etc.) are modeled over the life of the mission by the project and are used to generate requirements for the mission subsystems, including instruments (for example, the TID is 14.9 (krad-Si) at the 95% confidence level for 100 mils of spherical aluminum shielding). This includes possible Destructive Single-Event Effects. For Lucy, these requirements are contained within the Lucy Environmental Requirements Document (ERD). Electronic components and shielding are then defined in terms of meeting those requirements with margin. Some Single Event Effects will require power cycling, which is included in the mission design. Parity bits are included in the data transmission to the and spacecraft which enables a level of Error Detection and Correction (EDAC) in the image data. During encounters, data is transmitted to the spacecraft memory as soon as possible, typically within hours to a few days. It remains stored on L'Ralph as well. Data transmission to the ground depends on data rate and DSN availability and can take up to several months.

In addition, to ensure that L'Ralph is robust, almost all of the electronics are redundant. As illustrated in Fig. 6, L'Ralph can operate on two separate sides (side 1 or 2), the only common elements are the detector arrays themselves. For MVIC, the potential single point failure mode of the array is somewhat mitigated by having readouts on both sides of the serial output row in each CCD, so that if one 2500 pixel-wide side fails, the other might still be available. Although LEISA's use of 23 outputs corresponding to the twenty-three 64 row wide segments of the array is done to allow an acceptable frame rate, it also provides some redundancy. If any output should fail (or more, depending on the distribution), reasonably complete spectra may still be acquired. However, the likelihood that either MVIC or LEISA will have detector failures is extremely low.

MVIC always produces image data in CDS mode. LEISA "raw" mode is used to monitor the LEISA A/D converter offset level for each segment of the array. The same offset is used in both CDS and "raw" modes. The selectable offset compensates for voltage drifts in the analog signal train over the life of the mission, maintaining dynamic range without sacrificing signal resolution (increasing quantization noise).

For both MVIC and LEISA, the dominant noise source at low light levels is the system electronics noise, including array read noise. For MVIC this is about 20 e- ($\sim$ 200 μV) and for LEISA it is about 25 e- ($\sim$ 100 μV). The overall average gain for MVIC is about 28 e-/DN (Digital Number, or least significant bit), while for LEISA it is approximately 20 e-/DN.

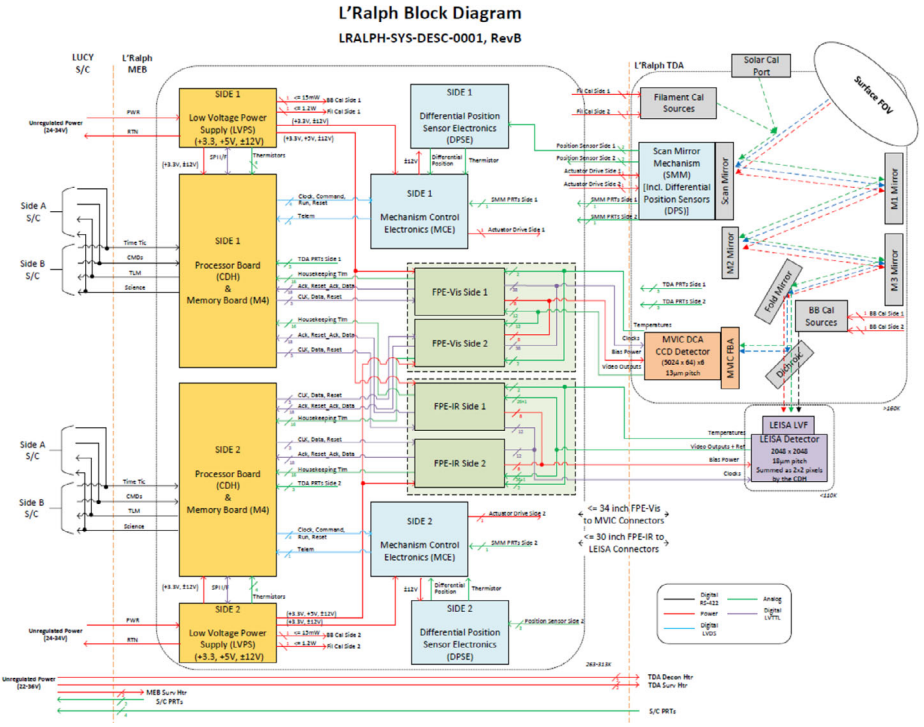

Fig. 6 Schematic of the L'Ralph electronics in the MEB and optical assembly in the TDA. Note that the system is fully redundant except for the MVIC and LEISA detectors, and the optical elements in the TDA. Both the MEB Side 1 and Side 2 electronics can be run off either the spacecraft Side A or Side B power interfaces

3.6 Pre-Launch Instrument Characterization

An extensive pre-launch program of performance verification measurements was carried out for L'Ralph at both the component level and the full instrument level. The component level characterization included measurements of the wavelength dependent quantum efficiency for the MVIC and LEISA array/filter assemblies and measurements of the wavelength dependence of the other optical elements (i.e., reflectance of the mirrors, transmission of the filters, and throughput of the beamsplitter). It also included measurements of the SMS scan rates and pointing accuracy as a function of the scan mirror sensor outputs, which allowed the development of command algorithms for accurate control of image motion scans. The primary performance characteristics determined in the instrument level tests were absolute radiometric calibration of the full system, spectral resolution, spatial resolution, signal to noise level, saturation level, calibration of the on-board calibration systems, optical pointing, and scattering. The stability of all these parameters was determined for both instrument sides, and under the thermal variations (LEISA detector temperatures of 90–115 K, MVIC detector temperatures of 155–200 K, TDA temperatures of 153–195 K) and voltage ranges (26–34 V) expected to be seen in flight. The directional characteristics of the solar calibration input were also measured, but only under ambient conditions.

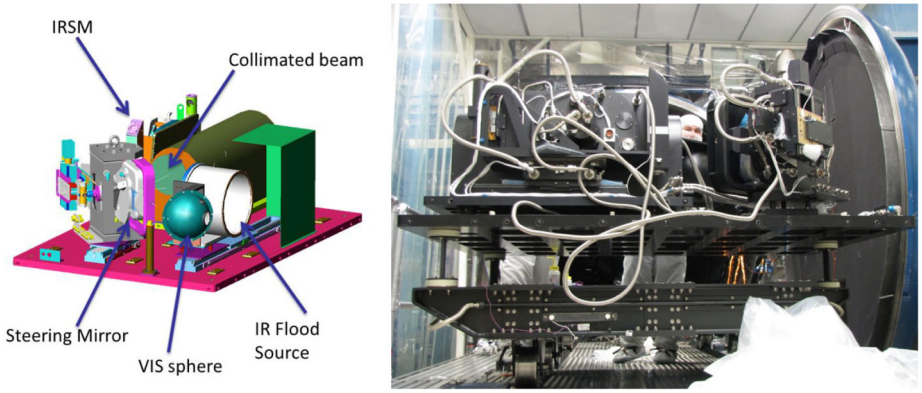

Fig. 7 (Left) Schematic of the in-chamber calibration system used to characterize L'Ralph performance. (Right) The calibration system being readied to enter the chamber

The instrument-level tests employed a system originally developed for calibrating the Thermal Infrared Sensor (TIRS) instrument on Landsat 8 and which has since been used for both the OSIRIS-REx OVIRS instrument and TIRS-2 on Landsat 9. This system consists of an infrared source module (IRSM) which illuminates collimating optics through a variety of apertures to simulate targets far removed from the output aperture. The output from the collimation source goes to a steering mirror that projects the beam onto the input of the instrument at a wide range of angles. This allows accurate location of the instrument's boresight. It also allows the off-axis scattering characteristics to be investigated. In addition to the IRSM, there are two NIST-traceable calibration sources in the calibration system, a visible integrating sphere providing visible and near IR radiation and a flood source providing light from the short-wave IR (SWIR) to the Far-IR. The entire calibration system, including the IRSM, the collimation system, the mirrors, the integrating sphere, and the flood source, goes into the chamber with the instrument. During testing, the components are cooled to near LN_2 temperatures so that unwanted thermal signal is minimized. In the chamber, the system may be configured such that light from an outside source can take the place of the IRSM and illuminate the collimating optics. This configuration is used, for example, to introduce the output of a grating monochromator into the system for spectral characterization. Figure 7 shows a diagram of the calibration system and a picture of it as it is about to enter the vacuum chamber.

3.7 Spectral Characterization

LEISA: The component-level spectral characterization of the LEISA focal plane assembly was performed at the Detector Characterization Laboratory at GSFC. This involved both determining the central wavelength of the pixels and measuring the spectral response function. Measurements were done in a temperature controlled dewar by illuminating the focal plane assembly with light from the output slit of a grating. For any wavelength, the halfwidth of the grating signal was always a factor of 4 (or more) less than the expected LEISA halfwidth. The grating output was collimated so that the entire unshielded detector array/filter assembly was lit, and multiple grating orders could be measured at each grating position. The central wavelength of each pixel was determined by stepping the lowest grating order about 10 pixels per step and fitting the cross-track weighted average maximum to a quadratic function at

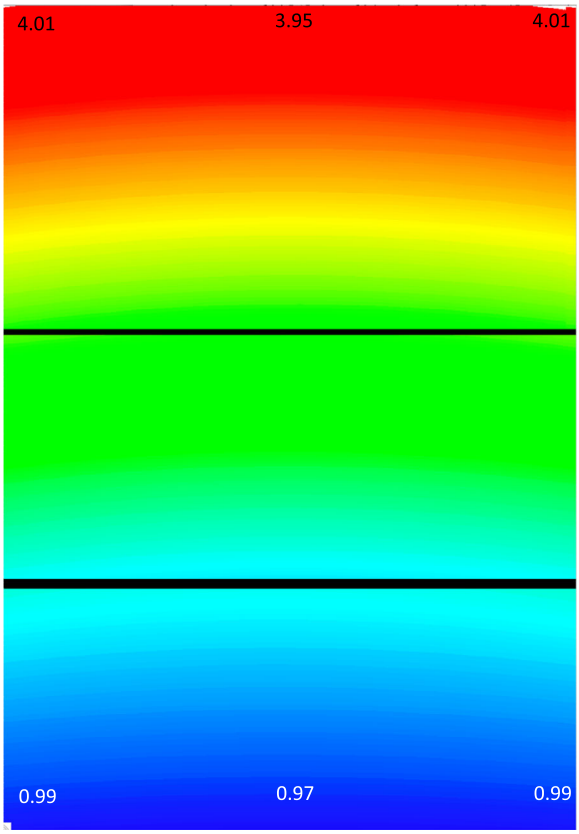

Fig. 8 Image showing the dependence of pixel central wavelength as a function of position on the LEISA focal plane. All 3 filter segments are shown, and the dark regions between them are the inter-filter bonds made with absorptive bonding material. The quadratic dependence in the cross-track direction is as expected from the filter deposition process

each step, and the along-track wavelength change to a linear function in each filter segment over all steps. The spectral response was determined every 40 to 60 rows in the along-track direction by stepping the grating such that about 8 samples were obtained over the FWHM, and 20 samples were obtained overall, As shown in Fig. 8, the central wavelengths cover more than the required 1 – 3.8 μm range over the 23 detector outputs that are being used for LEISA. The FWHM obtained at the along-track sampled regions are given in Table 3 and meet the $\leq$ 10 nm requirement for 1 – 3.4 μm. The spectral results were checked at several locations during instrument level TVac testing. Figure 9 shows an example of a spectral response curve measured during TVac at about 1.8 μm. As expected from the filter models developed by VIAVI, the spectral response near the central wavelength drops at close to a Gaussian rate as a function of wavelength displacement from the peak. These high spectral resolution measurements are not appropriate to determine the full out-of-band (OOB) performance because the signal generated by a narrow spectral band source far from the central wavelength would not generate sufficient signal. To determine the full out-of-band spectral performance, the set of broader filters used to measure the QE of the unfiltered detector were used to measure the spectral response of the filtered detector at wavelengths more than 10 HWHM (i.e. $<$ 50 nm) from the central wavelength. The summed OOB from the measurements was always $<$ 3%.

MVIC: As with LEISA, the initial spectral characterization of the MVIC components was performed by the component providers; STA Inc measured the spectral response of

Table 3 LEISA spectral resolution (FWHM) as a function of wavelength for a row near the center of the array. Note that, as shown in Fig. 8, there is some wavelength curvature in the columns perpendicular to this row, the resolution does not vary significantly

Center Wavelength (nm)	Pixel	Bandwidth FWHM (nm)
1008.8	1692	6.3
1111.3	1625	6.3
1213.5	1560	6.3
1314.4	1496	6.3
1415.9	1432	6.5
1516.9	1368	6.7
1616.5	1305	7.1
1612.3	1241	5.8
1710.1	1202	6.2
1812.5	1161	6.6
1910.9	1122	6.9
2014.3	1081	7.3
2113.1	1042	7.7
2211.7	1003	8.0
2310.8	964	8.5
2414.9	923	9.0
2513.9	884	9.1
2611.3	845	9.2
2611.3	799	8.8
2714.1	757	9.4
2814.1	716	9.7
2914.6	675	9.7
3012.3	635	9.7
3112.5	594	9.9
3210.8	553	10.0
3313.9	512	9.9
3414.7	471	9.8

the CCDs every 10 nm over the 300 to 1000 nm range and VIAVI Solutions measured the filer response every 0.5 nm over the same range. These were used to model the expected performance of the focal plane. The modeled responses were verified at the focal plane assembly level at SwRI and at the instrument level during TVac testing at Goddard. Figure 10 shows the instrument level spectral response curves for the MVIC bands.

3.8 Image Quality and Enclosed Energy

As noted in Table 1, the image quality requirements for both LEISA and MVIC are defined in terms of enclosed energy as a function of distance from the center of a pixel. This is a measure of how much signal is contributed by an area outside the IFOV of the pixel. For example, in the MVIC requirements shown in Table 1, a 91% enclosed energy at 168 μrad means that 9% of the pixel's signal comes from the region more than that 84 μrad from

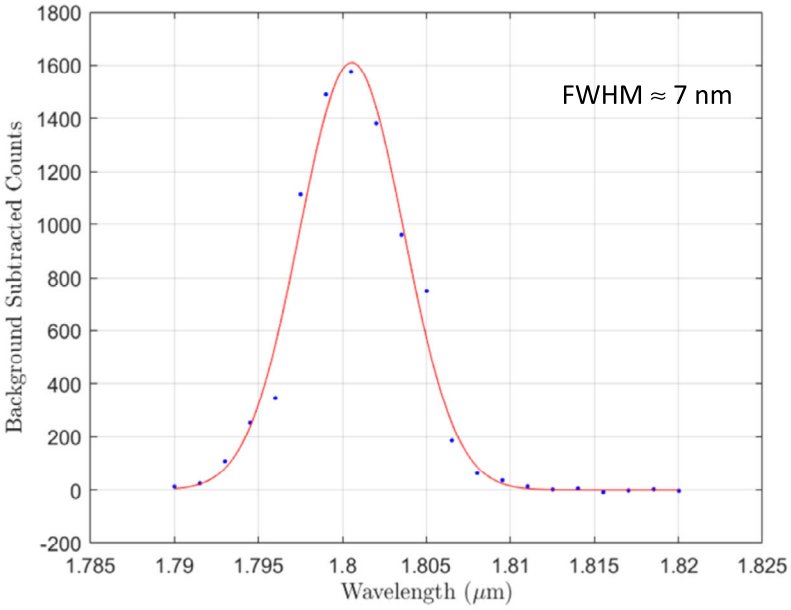

Fig. 9 Plot of the spectral band shape for a pixel near the cross-track center of the LEISA array. These data were obtained during Tvac testing at the instrumnet level and agree well with the results shown in Table 3. This is only displaying data obtained for measuring the FWHM

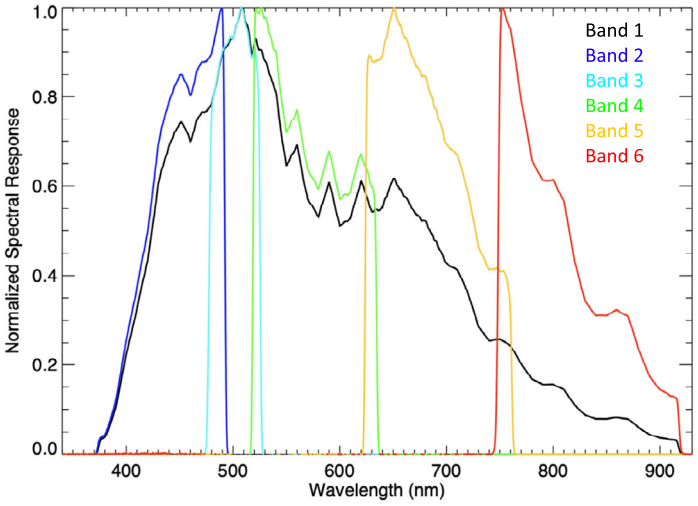

Fig. 10 Image showing the normalized spectral response for each of the MVIC channels. These were originally modeld as the product of measured spectrally dependent CCD QE, filter transmittance, mirror reflectances and dichroic filter transmittaance. The model was verified at the focal plane assembly level at SwRI and at the instrument level during TVac testing

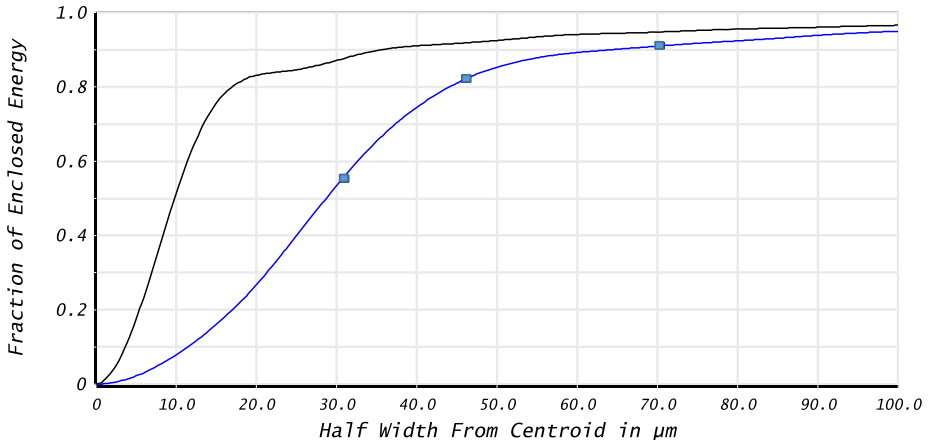

Fig. 11 (Top line) Graph of the enclosed energy fraction for a diffraction limited model of the L'Ralph optical system on the LEISA focal plane at a wavelength of 3.4 µm. The X-axis is in terms of distance from the center of a pixel in the center of the 3.4 µm spectral column. It may be converted to angular distance by multiplying by (80 µrad/36 µm). (Bottom line) Graph of the model degraded by introducing a wavefront error (WFE) term so that the performance as a function of distance meets the requirements as shown by the blue squares. The WFE was 840 nm RMS. For MVIC, the WFE error used to model the requirements was 245 nm

the center of the 28.8 µrad × 28.8 µrad MVIC IFOV. The enclosed energy measurements were done at the instrument level using collimated targets of various angular sizes which illuminated the entrance aperture and formed images on the focal plane. The change in the measured signal at the central pixel as a function of target size was compared to a model of the optical system that degraded the diffraction limited enclosed energy performance to the level of the required enclosed energy performance by including a wavefront error component in the model. In other words, if the instrument performance behaved as the model does, it would meet the requirements. The model process is illustrated in Fig. 11, which shows a comparison of the diffraction limited performance to the somewhat degraded required performance for pixels at the long-wavelength end of the LEISA spectral range. Using the model means that ratios of the observations made at smaller angular sizes to the observation at the maximum angular size may be used to verify requirements, and the maximum angular size does not have to have an enclosed energy of 100%. Note that the modeling also allows us to interpolate the required performance to measured target sizes that are not specified in the requirements. The actual measured performance is being compared to the requirements. This methodology was approved by several independent review teams.

LEISA: The enclosed energy measurements for the LEISA focal plane were made during TVac using the IRSM using targets of 50, 70, 141, 188, 282, and 800 µrad. For targets larger than 800, the intensity variation over the exposed area is affected by the spectral change over the more than 20 pixels, as well as the change arising from the optical system performance. In other words, for targets larger than 800 µrad, the shape of the image is affected by the spectral distribution of the source illuminating the target and thus is not uniform. Therefore, the largest target used in verifying the spatial response by the ratios of the central pixel intensity was 800 µrad. Note that the requirements for the LEISA enclosed energy performance are specified for the observations that are done to meet Level 1 requirements, which are made with the 2 × 2 superpixels, where the IFOV is 80 µrad.

Table 4 Ratio of enclosed energy as a function of target size to the 800 μrad enclosed energy for the measured and modeled LEISA focal plane

Size (μrad)	Measured Fraction	Modelled Fraction	Ratio
50	0.107	0.051	2.1
70	0.289	0.099	2.9
141	0.618	0.399	1.5
188	0.867	0.596	1.5
282	0.957	0.788	1.2

Table 5 Ratio of enclosed energy as a function of target size to the 435 μrad enclosed energy for the measured and modeled MVIC focal plane. The modeled performance is adjusted to the MVIC required level by including a 245 nm RMS WFE

Size (μrad)	Measured Fraction	Modelled Fraction	Ratio
27	0.176	0.153	1.2
43	0.324	0.328	1.0
65	0.650	0.548	1.2
218	0.974	0.922	1.1

The results for the ratio of the enclosed energy as a function of distance to the enclosed energy at 800 μrad is shown in Table 4. As may be seen, LEISA in 2 × 2 mode easily meets its enclosed energy requirements, as the driver for the requirement is the MVIC focal plane.

MVIC: The enclosed energy measurements for the 28.8 μrad IFOV MVIC focal plane were made using targets of 27, 43, 65, 218, and 435 μrad. Since MVIC is the driver for the enclosed energy performance, it was decided that a source with a larger focal length than the 1-meter focal length of the TVac calibration system would be used to ensure the light was fully collimated, hence the measurements were made under ambient conditions using a source with a 2.8-meter focal length. The measurements were made in the panchromatic channel because the highest spatial resolution measurements will be made with that channel. Since MVIC only operates in TDI mode it was necessary to use the scan mirror to scan the target image along the focal plane at the same rate as the charge transfer occurred during the CCD readout. Hence the measured enclosed energy includes the contribution of errors in the scan rate and is very representative of what will be seen in actual usage. The results obtained at ambient were verified in Tvac by carrying out focus scans which gave the same shape as was seen at ambient.

The results for the ratio of the enclosed energy as a function of distance to the enclosed energy at 435 μrad is shown in Table 5. As may be seen, MVIC meets or exceeds its enclosed energy requirements at the measured target sizes. These measurements were made at a TDA temperature of ∼175, near the midpoint of the expected TDA temperature range. Focal point measurements made at the upper and lower TDA temperature limits indicated that the focal point moved by ∼ 30 microns in the focus direction over the full field of view, which, for an f/6 beam corresponds to a broadening of ∼ 5 microns, which, when convolved with the 25 micron diameter of the FWHM, produces a negligible change of enclosed energy with temperature over the full field of view. Note that, since the diameter of the LEISA 2 × 2 superpixel FWHM is about 60 microns, the effect on LEISA is even smaller.

3.9 Radiometric Calibration and Signal-to-Noise Ratio (SNR)

As noted above, the pre-launch absolute radiometric calibration of the MVIC and LEISA components of L'Ralph was carried out using the visible-NIR integrating sphere and the IR flood source that are contained within the TVac calibration system. Both sources are NIST calibrated to better than 2% accuracy. Various settings of the temperature of the IR flood source and the aperture of the integrating sphere are used to get a range of radiances that are representative of the signal that will be seen from the Trojans over the range of solar distances, phase angles, and inherent reflectance values of the objects. These data were used to determine calibration coefficients for the detector elements. The calibration coefficients were found to be stable over the voltage and temperature ranges defined above. The resulting SNRs for LEISA and MVIC for the driving case of Polymele are described below.

LEISA: For all the Trojans the assumed reflectance range is 0.04 to 0.4 for all LEISA wavelengths. Under the assumption that the reflectance changes by 0.04 magnitudes/degree as a function of phase angle, this corresponds to an I/F range of 0.0019 to 0.019 for the Level 1 observations at Polymele which has the highest phase angle (82°) and, at 5.7 AU, is also the Trojan furthest from the sun that Lucy will visit. To obtain radiances consistent with these parameters the integrating sphere with varying apertures was used for wavelengths $<$ 2.2 μm and the flood source at several temperatures (345 K, 315 K, 275 K, and 225 K) was used for wavelengths $>$ 2.2 μm. Encounter design has limited the time available to do this observation to 800 sec, so for the 1 to 3.4 μm spectral range, this allows an integration time of 1.2 seconds to complete a scan of the 500 superpixels across the target. Figure 12 shows the SNR observed for the I/F of 0.0019. Note that this shows both superpixeled SNRs and non-superpixeled SNRs. Since this is for the required 70 nm Full Width tenth Maximum (FWTM) spectral resolution, pixels are summed in the spectral range. The spectral sampling is always 5 nm or less, so at least 14 pixels are summed in the spectral direction. As can be seen, LEISA easily meets the required SNR over the 1 to 3.4 μm spectral range even without superpixeling. With superpixeling, it meets the requirements over essentially the full spectral range covered by LEISA. Under these conditions there is no saturation for an I/F of 0.019. Because scans are done using the SMM and it takes less than 22 seconds to transition from 1 scan to the next, scans covering the full wavelength range will typically be done in two segments. The first will cover from 0.95 to about 2.6 microns and the second will cover from 2.6 to 3.9 microns. Since the intensity is greater at the shorter wavelengths, the second segment can be done at a rate about 3 times slower than the first (while still maintaining the overall time of the scan). This will improve the quality of the observation.

For Level 2 observations near close approach at near 0 phase angle LEISA will saturate at wavelengths $<$ 2.7 micron for an I/F of 0.4 at the shortest integration time for reading out 512 cross-track pixels (0.38 seconds). There are two simple ways around this, though: 1) if only 122 cross-track pixels are read out, the integration time can be reduced to 0.1 sec and no wavelengths saturate or 2) only data at wavelengths $>$ 2.7 microns is taken. Which solution is taken will depend on in-flight data and the science goal of the observation.

MVIC: For all the Trojans the assumed reflectance range is 0.03 to 0.4 for all MVIC channels. Under the assumptions above this corresponds to an I/F range of 0.0014 to 0.019. To obtain radiances consistent with these parameters the integrating sphere with varying apertures was used for all MVIC channels, since the flood source cannot be set to a high enough temperature to produce sufficient radiance in any channel. The encounter requirements are that one must be able to obtain an SNR $>$ 25 when scanning a 130 mrad target in the pan band in $<$ 45 seconds (a scan rate of 2900 μrad/sec or greater) and an SNR $>$ 25 in all the color channels when scanning a 130 mrad target in $<$ 180 seconds (a scan

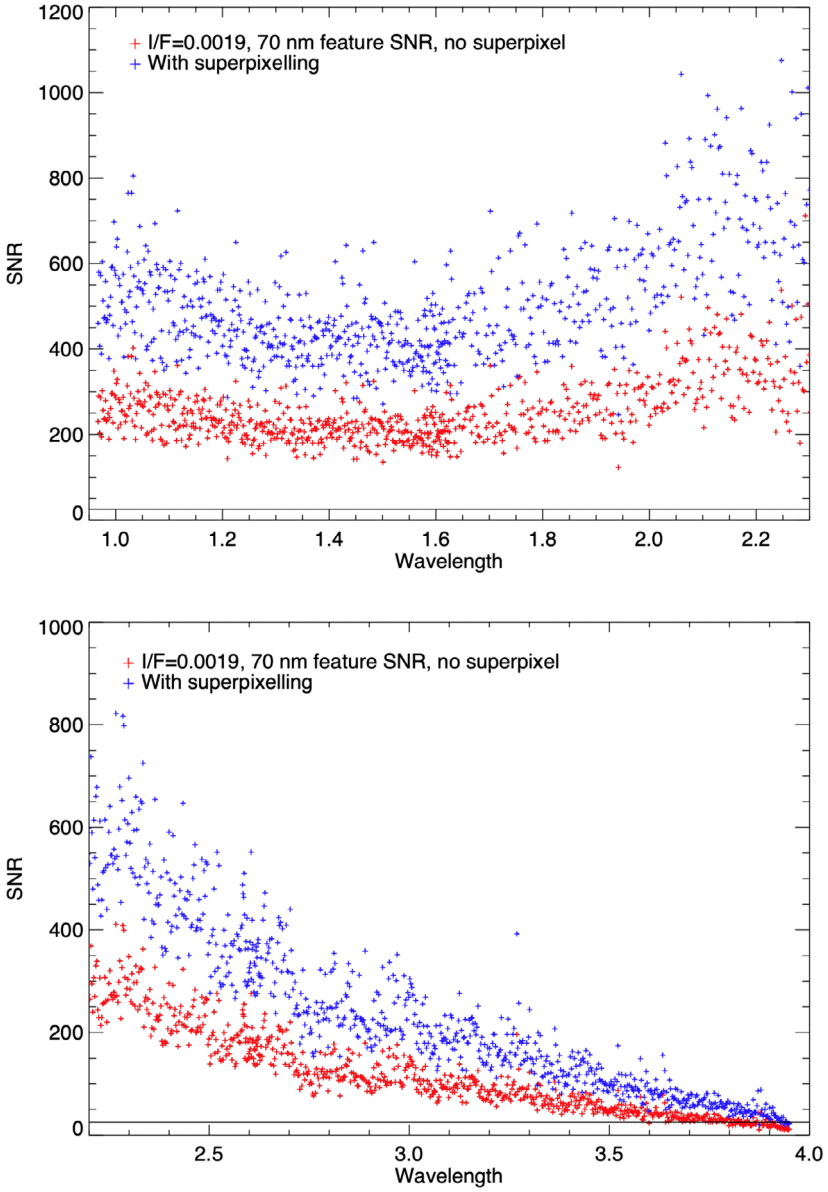

Fig. 12 SNR ratio for an I/F of 0.0019 at a heliocentric distance of 5.7 AU for a FWTM of 0.07 nm and a 1.2 second integration time. The requirement is that it must be above 25 for all wavelengths from 1 to 3.4 μm

rate of 800 μrad/sec or greater when taking the FOV between the MVIC channels into account). Table 6 shows the average SNR observed for an I/F of 0.0014 for a pan scan rate of 2900 μrad/sec using 32 TDI rows and a color channel scan rate of 800 μrad/sec also with 32 TDI rows in each channel. As may be seen from the table, the SNR requirement is easily met for all channels. In fact, the same results would be obtained for a 1600 μrad/sec color scan using 64 TDI rows. The actual scan operations remain to be determined from in-flight

Table 6 SNR for MVIC channels at 5.7 AU for I/F = 0.0014. The scan rate for pan is 2900 μrad/sec. The scan rate for the color channels is 800 μrad/sec. All cases use 32 TDI rows

BAND	AVERAGE SNR
pan	78.6
Violet	80.6
Green	60.2
Orange	133.4
Phyllosilicate	86.4
Near IR	32.9

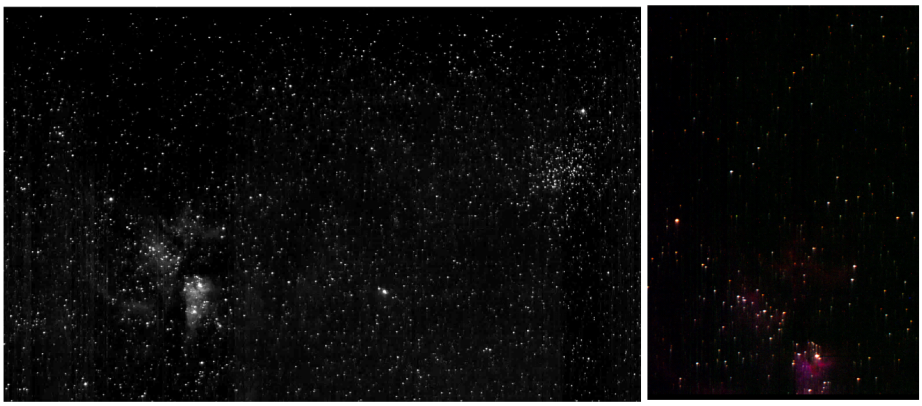

Fig. 13 Left; MVIC pan image showing the Wishing Well star cluster and a nebula. Right; a colorized version of the nebula obtained using data from the MVIC Green, Orange, and Phyllosilicate color channels during the same scan

observations. Note that, for the color scans shown in Table 6, there would be saturation in channel 4 for I/F = 0.019. This can easily be eliminated while still easily meeting the SNR > 25 requirement by reducing the number of TDI rows for this channel to 16.

For Level 2 observations near closest approach the color scans can be done using the fastest scan rate of 4000 μrad/sec and 4-8 TDI rows (depending on the band) to avoid saturation for I/F = 0.4 (even at 5.2 AU), however, the pan band would saturate for I/F > 0.15, even at TDI 4. There is no strong driver for obtaining pan scans at closest approach.

3.10 In-Flight Calibration Data

The Lucy Mission launched on October 16, 2021. Since its launch, L'Ralph has obtained data during a functional test done at approximately Launch + 20 days (L+20 days), calibration measurements done at approximately L+4 months and L+7 months, and a series of observations of the Earth and the Moon done during the Earth Gravity Assist (EGA-1) approximately 12 months after launch. The L+20 days L'Ralph test only verified that the operational parameters (voltages, currents, timing, etc.) were as expected. No images were obtained. The L+4 and L+7 month data collections included MVIC scans of M6 (the Butterfly Cluster, MGC 6405), M7 (NGC 6475) and the Wishing Well (NGC 3532). Figure 13 shows an example of a data obtained from the Wishing Well. The M6/M7 and Wishing Well scans were done at five different cross track positions to determine if there was a dependence of the radiometry on the placement of the image. The measurements did not indicate

Table 7 FWHMs in terms of number of pixels derived from stellar scans for all MVIC channels. The top row shows the results of fitting the two-dimensional PSF to a Gaussian function with a single variable (σ). The bottom row shows the results of fitting the same PSFs to a Gaussian function with two variables (σx and σy). The FWHM given in the bottom row is the geometric average $(\sigma x * \sigma y)^{1/2}$. To obtain the FWHM in terms of μrad, the numbers given above are multiplied by the IFOV (28.8 μrad)

	Pan	Violet	Green	Orange	Phyllo	NIR
# stars analyzed	**325**	**171**	**106**	**257**	**305**	**44**
FWHM: single variable	1.70 +/- 0.21	1.66 +/- 0.30	1.62 +/- 0.29	1.60 +/- 0.31	1.64 +/- 0.38	1.64 +/- 0.38
FWHM: two independent variables	1.66 +/- 0.24	1.62 +/- 0.29	1.59 +/- 0.27	1.56 +/- 0.29	1.61 +/- 0.35	1.61 +/- 0.35

there was any significant variation with the cross-track position and that the radiances obtained from the stars were consistent with pre-launch calibration. An analysis of the Point Spread Function (PSF) of the stellar observations also showed consistency of the FWHM measured in flight with the pre-launch value. Table 7 shows the results of fitting the measured 2-dimensional PSF to both a Gaussian with a single variable (σ) and a Gaussian with two variables (σx and σy) for numerous stars in the 6 MVIC channels. As may be seen from the table the FWHM obtained from the single variable fittings agrees well with the geometric average $(\sigma x * \sigma y)^{1/2}$ of the 2 variable fittings. That, and the fact that in the 2-D fits $\sigma x \sim = \sigma y$ indicates that the PSF is primarily driven by defocus at off-nominal temperatures and not by higher order asymmetric effects. (The nominal temperature ranges given in Sect. 3.6 are: LEISA detector temperatures of 90–115 K, MVIC detector temperatures of 155–200 K, TDA temperatures of 153–195 K. At times, during some in-flight observations, the TDA was at 215 K and/or MVIC was at 212 K.) The inflight results of a FWHM of $\sim$ 1.7 pixels ($\sim$50 μrad) agree well with the pre-launch MVIC enclosed energy results discussed above and presented in Table 5 and are consistent with the requirements. MVIC measurements made during L+7 also verified the pointing of the solar calibrator and provided the baseline intensity levels for comparison with future observations. MVIC measurements of the on-board filament calibration source intensities were consistent with pre-launch values. We note that, as expected for heliocentric distances less than about 3 AU, the temperature of the LEISA detector was too high to allow any stellar observations to be made without dark current saturation. LEISA solar and on-board calibration source measurements were also not possible for the same reason.

During EGA-1, MVIC scans of the Earth were done at 5 different cross-track positions. As expected, these observations were mostly saturated and did not provide any radiometric or extended source optical performance information. However, they were extremely useful in providing measurements of the scattering characteristics of L'Ralph. They have verified that, for the angular range of the observations to be made at the Trojans, scattering is significantly less than 1% and therefore is not an issue for the reflectance range specified in the requirements. MVIC color scans of the Moon did provide unsaturated images over most of the surface in the Violet, Green and NIR channels. The Phyllosilicate and Orange images are not saturated in the area near the terminator. Since the lunar scans were repeated at 5 cross-track positions, averages in the unsaturated regions allowed further verification that any dependence of signal level on cross-track location is accounted for in the pre-launch calibration. Figure 14 shows the calibrated radiance obtained in each of the 5 scans for the

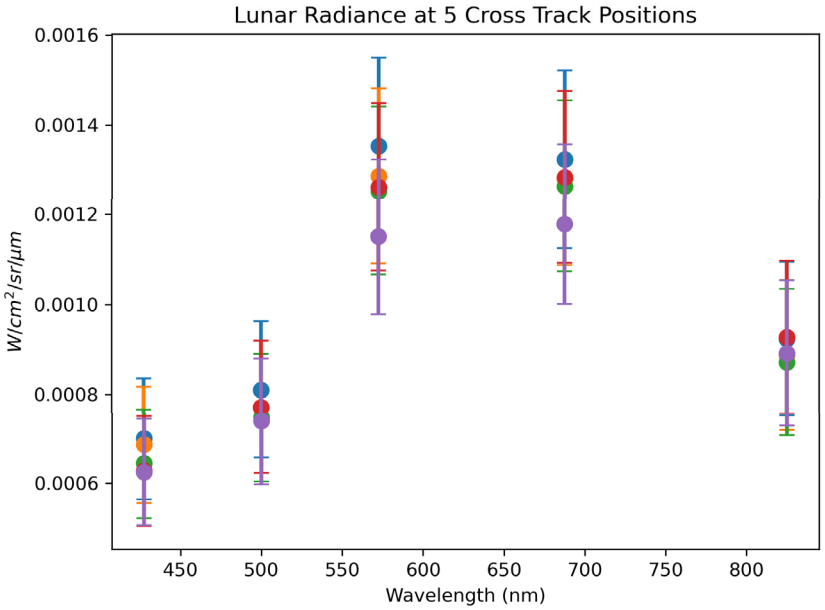

Fig. 14 Plot of the mean radiances obtained in an area near the terminator for each of the 5 MVIC color channels in each of the 5 lunar scans. The error bars represent the standard deviation over the area

5 MVIC color channels at an area near the terminator where none of the channels are saturated. As may be seen from the figure, in each channel the data at all 5 scan positions fall within the standard deviations, and there is no apparent dependence on what part of the array is used to obtain the data. The MVIC pan channel was still saturated in this region. Figure 15 shows a comparison between MVIC I/F data (based on pre-launch calibration) obtained in the Lunar Mare and Highlands regions, where none of the color channels were saturated, with the Moon Mineralogy Mapper (M3) reflectance data in those areas. The MVIC data is corrected to the incidence angle (i) = 30°, emissivity (e) = 0°, and phase (α) = 30° standard used by M3 (Green et al. 2011; Besse et al. 2013). As may be seen, the MVIC and M3 data agree well in these areas (the M3 data does not extend into the wavelengths of the MVIC Violet and Green channels). Figure 15 also shows a comparison between the MVIC data and the ROLO standard modeled data (Kiefer and Stone 2005) over the entire lunar surface (note that saturated areas are excluded from the MVIC data, which primarily affects the Phyllosilicate and Orange channels). The ROLO model does cover all MVIC channels. Once again, there is good agreement between the MVIC data and the standard.

Finally, during EGA-1, some unsaturated LEISA spectral observations of the Earth were made. This was made possible by three non-standard conditions. First, for several hours before the scans were done, the IPP could be pointed in a direction that minimized heating of the TDA and the focal plane due to radiation from the solar cells. While the scans could not be carried out in this orientation, this lowered the detector temperature to about 150 K before the scans were done. This is still about 40 K higher than the normal operating temperature at the Trojans, where heating from the solar cells will not be problematic. Second, the cross-track readout size of the LEISA detector was reduced from 512 pixels to 20 pixels, which allowed the minimum integration time to be reduced from 0.38 seconds to about 0.026 seconds. Of course, this significantly reduced the image size, but it meant that,

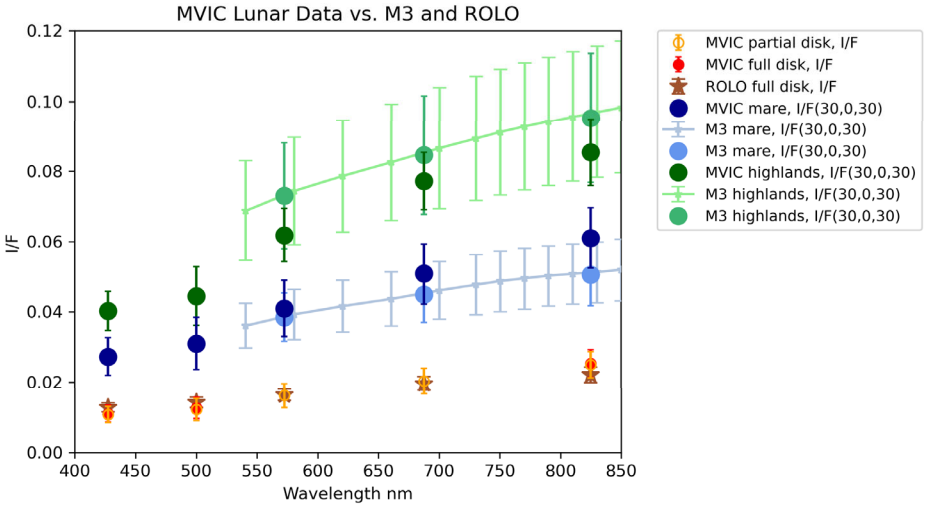

Fig. 15 An I/F comparison between MVIC data taken on the moon with appropriately spectrally sampled 1) ROLO global model data and 2) Moon Minerology Mapper (M3) reflectance data over the lunar Mare and lunar Highland areas where MVIC was not saturated in any channel. For the latter cases the MVIC data were corrected to the incidence angle (i) = 30°, emissivity (e) = 0°, and phase (α) = 30° standard used by M3. The ranges given in the comparison between the M3 and MVIC data represent the range of I/F observed in the Mare and Highland areas. For the Rolo comparisons the MVIC data are not corrected for (i.e., α) and the MVIC uncertainties are the standard deviations over the area observed. The ROLO uncertainties are those produced by the model. Note that the M3 data do not extend to the wavelengths of the two shortest wavelength MVIC channels, but the ROLO model does

even though the detector dark current was several orders of magnitude higher than it will be at the Trojans, data not saturated by dark current could be obtained. Finally, the much higher signal produced by the Earth than will be produced by the Trojans was sufficient to produce a measurable signal in the much shorter integration time. Figure 16 shows an example of a spectrum obtained in a region near Australia. As may be seen in this figure, the LEISA spectrum does show the expected structure for Earth. Although, because of the non-standard condition under which these data were obtained, they cannot be used to verify radiance levels etc., they do indicate that the LEISA hyperspectral imager is working.

3.11 Conclusion

This paper describes the design, operation, and performance of L'Ralph, a highly capable, very flexible, Vis/NIR multispectral imager/SWIR hyperspectral imager flying on the Lucy mission to the Trojan asteroids in Jupiter's orbit. L'Ralph consists of a telescope feeding two focal planes, the visible/NIR MVIC imager and the LEISA. MVIC will provide very sensitive, high fidelity, panchromatic and multi-spectral maps of the Trojans at a spatial resolution of 1.5 km/FWHM or higher over most of the surface and 0.6 km/FWHM over a good fraction of it. LEISA will provide full hemispheric, SWIR, spectral maps with spatial resolutions of 1-5 km/FWHM or better. These will be used to accurately characterize the surface composition, and variations associated with fresh surface regions in particular. At near closest approach, MVIC can obtain images with spatial resolutions on the order of fifty to one hundred meters, while LEISA can measure spectra at the 100 to 200 m spatial scale. L'Ralph has been extensively tested at the component and full instrument level and its in-flight operation has verified that MVIC meets all its performance requirements with margin.

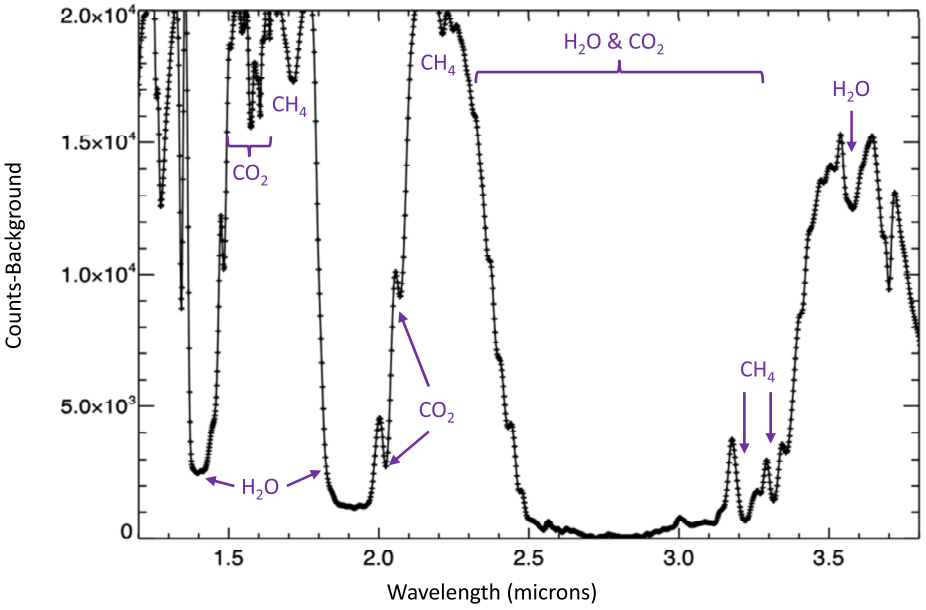

Fig. 16 Spectrum of the Earth obtained by LEISA near the northeast coast of Australia. Expected spectral features are evident

(LEISA requirements have not been verified in-flight because, as expected, for heliocentric distances of 3 AU or less its focal plane has not cooled sufficiently to allow operation at the conditions that will exist at the Trojans. However, observations of Earth taken at warmer-than-optimal operating temperatures indicate LEISA is operating nominally.) L'Ralph will provide a wealth of information on the geology, composition, morphology and thermal characteristics of the Trojan objects. The data it produces during its flybys will shed new light on the formation and evolution of our solar system.

Acknowledgements The authors would like to thank the entire L'Ralph support teams at GSFC and SwRI (San Antonio) for their untiring efforts in making L'Ralph a reality. The contributions of VIAVI Solutions, STA Inc, TIS, NuTek, Coherent/Tinsly, Jackson and Tull, Newton Engineering and Product Development, Big Head Endian LLC, Markury Scientific and Blue Line Engineering are also gratefully acknowledged. The authors would also like to thank the PI office at the Southwest Research Institute, the Project Office at GSFC, the Program Office at MSFC and NASA HQ for their support.

Declarations

Competing Interests The authors declare that they have no competing interests.

References

Beletic JW et al (2008) Teledyne Imaging Sensors: infrared imaging technologies for astronomy and civil space. In: Proc. SPIE 7021, High energy, optical, and infrared detectors for astronomy III, vol 70210H

Besse B, Sunshine J, Staid M, Boardman J, Pieters C, Guasqui P, Malaret E, Mclaughlin S (2013) A visible and near-infrared photometric correction for Moon Mineralogy Mapper (M3). Icarus 222:229–242

Brown ME (2016) The 3-4 μm spectra of Jupiter Trojan asteroids. Astron J 152:159

Buie M, Keeny B, Levison H, Olkin C, Lucy Occultations Team (2022) Shape and duplicity of Lucy Mission target Polymele from occultation observations. AAS DPS 54, London, Ontario CA

Campins H, Hargrove K, Pinilla-Alonso N, Howell ES, Kelley MS, Licandro J, Mothe-Diniz T, Fernandez Y, Ziffer J (2010) Water ice and organics on the surface of the asteroid 24 Themis. Nature 464:1320–1321

Cruikshank DP et al (2008) Hydrocarbons on Saturn's satellites iapetus and phoebe. Icarus 193:334–343

Dalle Ore CM, Cruikshank DP, Clark RN (2012) Infrared spectroscopic characterization of the low-albedo materials on Iapetus. Icarus 221:735–743

Green RO, Pieters C, Mouroulis P, Eastwood M, Boardman J, Glavich T, Isaacson P, Annadurai M, Besse S, Barr D, Buratti B, Cate D, Chatterjee A, Clark R, Cheek L, Combe J, Dhingra D, Essandoh V, Geier S, Goswami JN, Green R, Haemmerle V, Head J, Hovland L, Hyman S, Klima R, Koch T, Kramer G, Kumar ASK, Lee K, Lundeen S, Malaret E, McCord T, McLaughlin S, Mustard J, Nettles J, Petro N, Plourde K, Racho C, Rodriquez J, Runyon C, Sellar G, Smith C, Sobel H, Staid M, Sunshine J, Taylor L, Thaisen K, Tompkins S, Tseng H, Vane G, Varanasi P, White M, Wilson D (2011) The Moon Mineralogy Mapper (M^3) imaging spectrometer for lunar science: instrument description, calibration, on-orbit measurements, science data calibration and on-orbit validation. J Geophys Res, Planets 116:E10

Kiefer HH, Stone TC (2005) The spectral irradiance of the Moon. Astron J 129:2887–2901

Leland JE, Arecchi AV (1995) Analysis of spectralon® material for use in on-board calibration systems for the medium resolution imaging spectrometer (MERIS). SPIE, vol 2475

Levison HF, Olkin CB, Noll KS, Marchi S, Bell JF III, Bierhaus E, Binzel R, Bottke W, Britt D, Brown M, Buie M, Christensen P, Emery J, Grundy W, Hamilton VE, Howett C, Mottola S, Pätzold M, Reuter D, Spencer J, Statler TS, Stern SA, Sunshine J, Weaver H, Wong I (2021) Lucy mission to the Trojan asteroids: science goals. Planet Sci J 2:171

Levison HF et al (2024) Lucy science and mission overview. Space Sci Rev 220

Loose M, Beletic J, Blackwell J, Garnett J, Wong S, Hall D, Jacobson S, Rieke M, Winters G (2005) The SIDECAR ASIC: focal plane electronics on a single chip. In: Proc. SPIE 5904, Cryogenic optical systems and instruments XI, 59040V

Noll KS, Brown ME, Weaver HA, Grundy WM, Porter SB, Buie MW, Levison HF, Olkin C, Spencer JR, Marchi S (2020) Detection of a Satellite of the Trojan asteroid (3548) Eurybates—a Lucy mission target. Planet Sci J 1:44

Olkin CB, Levison HF, Vincent M, Noll KS, Andrews J, Gray S, Good P, Marchi S, Christensen P, Reuter D, Weaver H, Pätzold M, Bell JF III, Hamilton VE, Dello Russo N, Simon A, Beasley M, Grundy W, Howett C, Spencer J, Ravine M, Caplinger M (2021) Lucy mission to the Trojan asteroids: instrumentation and encounter concept of operations. Planet Sci J 2:172

Olkin C B et al (2024) Mission design and concept of operations for the Lucy mission. Space Sci Rev 220

Reuter DC, Stern SA, Scherrer J, Jennings DE, Baer J, Hanley J, Hardaway L, Lunsford A, McMuldroch S, Moore J, Olkin C, Parizek R, Reitsma H, Sabatke D, Spencer J, Stone J, Throop H, Van Cleve J, Weigle GE, Young LA (2008) Ralph: a visible/infrared imager for the new horizons Pluto/Kuiper belt mission. Space Sci Rev 140:129–154

Reuter DC, Simon AA, Hair J, Lunsford A, Manthripragada S, Bly V, Bos B, Brambora C, Caldwell E, Casto G, Dolch Z, Finneran P, Jennings D, Jhabvala M, Matson E, McLelland M, Roher W, Sullivan T, Weigle E, Wen Y, Wilson D, Lauretta DS (2018) The OSIRIS-REx Visible and InfraRed Spectrometer: spectral maps of the asteroid Bennu. Space Sci Rev 214:54

Rivkin AS, Emory JP (2010) Detection of ice and organics on an asteroidal surface. Nature 464:1322–1323

Rosenberg KP, Hendrix KD, Jennings DE, Reuter DC, Jhabvala MD, La AT (1994) Logarithmically variable infrared etalon filters. In: SPIE proceedings, Optical thin films IV: new developments, San Diego, vol 2262, pp 25–27

Simon AA, Reuter DC, Gorius N, Lunsford A, Wind G, Cosentino RG, Lauretta D, The OSIRIS-REx Team (2018) In-flight calibration and performance of the OSIRIS-REx visible and IR spectrometer (OVIRS). Remote Sens 10:1486

Takir D, Emery JP (2012) Outer main Belt asteroids: identification and distribution of four 3- μm spectral groups. Icarus 219:641–654

Takir D, Emery JP, McSween HY, Hibbitts CA, Clark RN, Pearson N, Wang A (2013) Nature and degree of aqueous alteration in CM and CI carbonaceous chondrites. Meteorit Planet Sci 48:1618–1637